

# Explainable 2D Vision Models for 3D Medical Data

Alexander Ziller<sup>1</sup>, Alp Güvenir<sup>1</sup>, Ayhan Can Erdur<sup>1,3</sup>, Tamara T. Mueller<sup>1</sup>, Philip Müller<sup>1</sup>, Friederike Jungmann<sup>1,2</sup>, Johannes Brandt<sup>1</sup>, Jan Peeken<sup>3</sup>, Rickmer Braren<sup>2</sup>, Daniel Rueckert<sup>1</sup>, and Georgios Kaissis<sup>1,2,4</sup>

<sup>1</sup> AI in Medicine and Healthcare, Technical University of Munich, Einsteinstr. 25, 81675 Munich

<sup>2</sup> Institute for diagnostic and interventional Radiology, Technical University of Munich, Ismaningerstr. 22, 81675 Munich

<sup>3</sup> Department of Radiation Oncology, Technical University of Munich, Ismaningerstr. 22, 81675 Munich

<sup>4</sup> Institute for Machine Learning in Biomedical Imaging, Helmholtz Zentrum Munich, Ingolstädter Landstr. 1, 85764 Munich  
{alex.ziller}@tum.de

**Abstract.** Training Artificial Intelligence (AI) models on three-dimensional image data presents unique challenges compared to the two-dimensional case: Firstly, the computational resources are significantly higher, and secondly, the availability of large pretraining datasets is often limited, impeding training success. In this study, we propose a simple approach of adapting 2D networks with an intermediate feature representation for processing 3D volumes. Our method involves sequentially applying these networks to slices of a 3D volume from all orientations. Subsequently, a feature reduction module combines the extracted slice features into a single representation, which is then used for classification. We evaluate our approach on medical classification benchmarks and a real-world clinical dataset, demonstrating comparable results to existing methods. Furthermore, by employing attention pooling as a feature reduction module we obtain weighted importance values for each slice during the forward pass. We show that slices deemed important by our approach allow the inspection of the basis of a model’s prediction.

## 1 Introduction

Deep learning has emerged as a promising technology in medical imaging, offering the potential to automate and enhance various aspects of patient care. While most computer vision applications focus on 2D image analysis such as photographs, medical imaging stands out by capturing true 3D voxel images through techniques like computed tomography (CT) or magnetic resonance imaging (MRI). Adapting existing 2D models to work with 3D data is not straightforward, as it poses challenges in obtaining high-quality pre-trained weights from large datasets [14]. Additionally, training 3D models requires significantly more computational and memory resources compared to their 2D counterparts [16]. In response to these

considerations, researchers have explored 2.5D architectures as a compromise, aiming to combine the benefits of strong pre-training with reasonable computational requirements while leveraging the inherent nature of 3D volumes. These 2.5D architectures often rely on recurrent neural networks (RNN) [10], e.g. long and short term memory units (LSTM) [8, 2, 17, 3].

In sensitive domains such as medical data analysis, it is essential to have trustworthy systems. One crucial requirement is the ability to understand the decision-making process. Deep learning models have often been criticised as “black-boxes”, where the input and output are observed, but the internal connections remain obscure. To address this concern, interpretability and explainability methods have been developed, e.g. Grad-CAM and its successors, for instance, allowing for retrospective inspection of these connections [12].

One of the remarkable advancements in deep learning is the introduction of attention mechanisms [13]. Originally developed for natural language processing, attention mechanisms have also demonstrated impressive performance in vision tasks [5]. These approaches are based on the intuition of “learning what is important” and thus prioritising the influence to the model’s prediction. This concept has also been extended to improve pooling operations [11], which are commonly applied as a maximum or averaging operation over large inputs in neural networks.

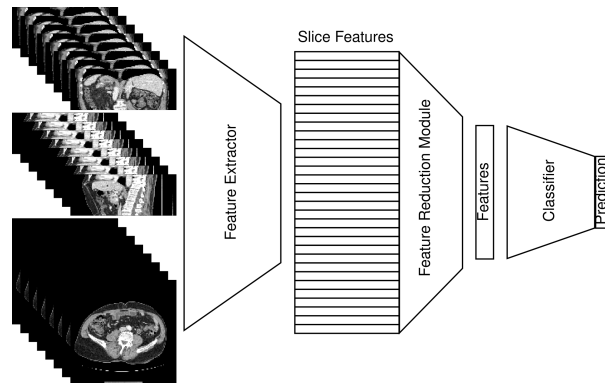


Fig. 1: Overview of our approach to convert a standard 2D vision architecture to obtain a 2.5D model. Example image stems from the MSD Liver dataset [1]

In this study, we introduce a simple template, that enables the conversion of arbitrary 2D architectures with intermediate feature representations into 2.5D architectures. To the best of our knowledge, this template aligns with the prevailing pattern followed by state-of-the-art (SOTA) architectures. Our proposed method offers several distinct advantages. Firstly, the computational overhead incurred by our 2.5D model is primarily determined by the feature reduction module. As a result, the additional computational requirements compared to a

2D model are minimised, allowing for efficient utilisation of computing resources. Secondly, our approach allows for the utilisation of strong pretrained weights that are readily available for 2D architectures. By leveraging these pretrained weights, we can effectively transfer the knowledge captured from large-scale 2D datasets to enhance the performance of our 2.5D models. Lastly, when employing attention pooling in our framework, we inherently generate an attention map during the forward pass. This attention map serves as an implicit explanation of the contribution of individual slices to the final prediction. By visualising the attention map, we gain insights into the important regions and slices that influence the model’s decision-making process, thereby enhancing the interpretability of our approach. Through our experimental evaluation, we demonstrate the efficacy of our template in improving both the performance and explainability of medical image analysis tasks. We will release our code upon acceptance of the manuscript.

*Prior work* There exist several lines of work, which approach 2.5D architecture designs [16, 10, 2, 3, 17]. Yang et al. [14] developed methods to make pretrained 2D architectures applicable to 3D images. They apply the convolutional filters along all three axes and thus create an artificial 3D kernel, which they term ACS-convolution. Similar to our approach this allows them to re-use information learned in the 2D domain, while keeping the number of parameters almost constant. The closest to our work is likely the work by Li et al. [9]. They combined 2D neural networks as feature extractors with transformer blocks for lesion detection. This allows to learn the attention over all slices of the 3D input and combines them into a single representation. However, transformers are computationally expensive and require significantly more memory, annihilating the advantage of 2D over 3D models. There are numerous methods to quantify the contribution of inputs to the output of a model. Most prominently, we note Grad-CAM [12] and its successors. However, most of them are based on retrospectively inspecting a model. Using attention pooling yields such a contribution quantification directly in the forward pass, making predictions inherently explainable.

*Our contributions* In this work we introduce an intuitive and versatile template for converting 2D to 2.5D models. Our approach involves applying the feature extraction part to each slice of a disassembled 3D scan and subsequently utilising a feature reduction module to condense the extracted features into a single representation. We experimentally benchmark our approach with different feature reduction modules on several benchmark dataset and a real-world clinical dataset. We demonstrate that our approach is at least on par with prior work and when using average pooling even outperforms other methods. Furthermore, we propose the usage of attention pooling as a feature reduction module, which allows to quantify the contribution of each slice to the prediction during the forward pass. We exemplify this on the task of classifying the presence of a tumour, where our model focuses not on the tumour itself, but on secondary effects, such as metastases or gallbladder congestion.

## 2 Methods

We leverage the prevalent structure commonly found in deep learning architectures, which consists of a feature extraction module followed by a classifier. Exploiting this pattern, we decompose the 3D image into 2D slices along all axes. These individual slices are then fed into the feature extraction component of the original network, resulting in the retrieval of  $H + W + D$  feature representations, where  $H$  represents the height,  $W$  denotes the width, and  $D$  signifies the depth of the 3D scan. To consolidate these feature representations into a single comprehensive representation, we employ a feature reduction module, as illustrated in Figure 1. This aggregated feature representation serves as the input to the subsequent classification module.

Among the various feature reduction techniques that we evaluate, attention pooling stands out as a notable approach. This method involves utilising a Multihead Attention layer [13], which takes query, key, and value inputs. Following the suggestion by Radford et al. [11], we employ the mean of all slice features as the query, while the key and value comprise the complete set of features. By doing so, our network is capable of estimating the significance of each feature and generating a weighted combination of the input features that best represents the input scan for a given task. Furthermore, this approach generates attention maps during the forward pass, providing insights into the contribution of each individual slice to the final feature representation. The resultant aggregated feature representation is then fed into the classification layer for prediction.

By adopting this framework, we aim to exploit the inherent advantages of both 2D and 3D architectures, leveraging the strong pretraining available for 2D models while processing the complete 3D volumes. The attention pooling mechanism not only facilitates feature reduction but also enhances the interpretability of our approach by implicitly generating attention maps. These attention maps shed light on the contribution of individual slices to the overall feature representation, aiding in the comprehension of the decision-making process of our model.

## 3 Results

### 3.1 Dataset

We use all 3D datasets from MedMNIST [15], which are real-world medical datasets that have been preprocessed and standardised to a resolution of  $28 \times 28 \times 28$ . They represent diverse medical AI problems and present distinct challenges with benchmark results available from previous work. For detailed information we refer to [15].

To showcase the clinical applicability of our approach, we incorporated an internal dataset of 1 625 abdominal CT scans, classifying the presence of pancreatic ductal adenocarcinoma (PDAC). Out of the total dataset, 867 patients were diagnosed with a tumour by a panel of medical experts, while the remaining 758 CT scans were obtained from patients with diagnoses unrelated to the pancreas, serving as the control group. All images encompass the relevant body regions and

Table 1: Benchmarking of our models on the MedMNIST3D datasets. AUC denotes the area under the receiver-operator curve, ACC the classification accuracy. #P denotes the number of trainable parameters of the model architecture in millions. The first part of the tables shows the results reported by Yang et al. [15]. The second part summarises the mean results over five runs of our experiments. The first three models of the second part are equivalent to the first part of the table. Last column shows the test results on the PDAC dataset from a single run.

|                    | Method      | #P [M] | MedMNIST 3D |        |          |         |        |         | PDAC  |       |
|--------------------|-------------|--------|-------------|--------|----------|---------|--------|---------|-------|-------|
|                    |             |        | Organ       | Nodule | Fracture | Adrenal | Vessel | Synapse |       |       |
| Results by [15]    | 3D-Conv     | 33.2   | AUC         | 99.6%  | 86.3%    | 71.2%   | 82.7%  | 87.4%   | 82.0% |       |
|                    |             |        | ACC         | 90.7%  | 84.4%    | 50.8%   | 72.1%  | 87.7%   | 74.5% |       |
|                    | 2.5D-Conv   | 11.2   | AUC         | 97.7%  | 83.8%    | 58.7%   | 71.8%  | 74.8%   | 63.4% |       |
|                    |             |        | ACC         | 78.8%  | 83.5%    | 45.1%   | 77.2%  | 84.6%   | 69.6% |       |
|                    | ACS-Conv    | 11.2   | AUC         | 99.4%  | 87.3%    | 71.4%   | 83.9%  | 93.0%   | 70.5% |       |
|                    |             |        | ACC         | 90.0%  | 84.7%    | 49.7%   | 75.4%  | 92.8%   | 72.2% |       |
| Approaches by [14] | 3D-Conv     | 33.2   | AUC         | 96.5%  | 58.1%    | 57.9%   | 80.7%  | 92.3%   | 61.9% | 98.4% |
|                    |             |        | ACC         | 77.8%  | 74.0%    | 43.4%   | 79.9%  | 93.8%   | 66.1% | 92.3% |
|                    | 2.5D-Conv   | 11.2   | AUC         | 96.3%  | 57.9%    | 49.1%   | 50.0%  | 55.9%   | 59.2% | 98.9% |
|                    |             |        | ACC         | 76.0%  | 73.3%    | 37.3%   | 76.8%  | 89.7%   | 69.7% | 94.5% |
|                    | ACS-Conv    | 11.2   | AUC         | 99.2%  | 79.0%    | 58.1%   | 79.1%  | 84.3%   | 61.5% | 99.4% |
|                    |             |        | ACC         | 89.7%  | 81.9%    | 43.8%   | 80.1%  | 91.0%   | 71.1% | 96.9% |
| Ours               | AveragePool | 11.2   | AUC         | 99.6%  | 86.9%    | 58.3%   | 87.0%  | 93.1%   | 83.7% | 99.3% |
|                    |             |        | ACC         | 91.4%  | 85.3%    | 43.3%   | 81.9%  | 88.7%   | 80.1% | 96.9% |
|                    | MaxPool     | 11.2   | AUC         | 99.2%  | 84.9%    | 57.6%   | 76.3%  | 84.3%   | 68.0% | 94.6% |
|                    |             |        | ACC         | 88.5%  | 84.7%    | 42.3%   | 79.9%  | 89.8%   | 72.2% | 90.2% |
|                    | LSTM        | 11.6   | AUC         | 99.4%  | 84.6%    | 56.1%   | 78.9%  | 88.3%   | 70.7% | 92.2% |
|                    |             |        | ACC         | 92.2%  | 82.3%    | 40.2%   | 76.3%  | 89.9%   | 72.0% | 78.8% |
| Transformer        | 55.3        | AUC    | 97.1%       | 67.3%  | 58.3%    | 65.9%   | 59.8%  | 62.7%   | 84.8% |       |
|                    |             | ACC    | 78.1%       | 80.8%  | 40.2%    | 76.8%   | 88.7%  | 73.4%   | 52.3% |       |
| AttentionPool      | 12.2        | AUC    | 99.5%       | 82.3%  | 58.8%    | 80.9%   | 91.4%  | 74.3%   | 98.1% |       |
|                    |             | ACC    | 92.0%       | 83.9%  | 42.7%    | 78.9%   | 91.8%  | 75.5%   | 92.9% |       |

were acquired following the same imaging protocol. We split this dataset into 975 CTs as train images and 325 for validation and testing each. We ensured that the distribution of classes in each subset is approximately equal. Additionally, all CT scans are resized to a standardised resolution of  $224 \times 224 \times 128$  voxels and clipped to an abdominal window of  $(-150, 250)$  Hounsfield units.

### 3.2 Baseline models

For our experiments we adopted a ResNet-18 [7] as the base architecture. Consistent with the approach by Yang et al. [15], we employed the framework by the same authors [14] to convert the model into 3D, 2.5D and ACS forms. Furthermore, we evaluated our template with various feature reduction modules. As simple baselines, we utilised average pooling and max pooling operations. The average pooling operation calculates the average of all feature representations, while the max pooling operation returns the maximum value for each position across all features. Additionally, we incorporated a simple learned module, the LSTM RNN, which aggregates the feature representations. We also tested a transformer architecture with eight heads, six encoder and decoder layers, following the approach of Li et al. [9]. Lastly, we showcased the effectiveness of using attention pooling as a feature reduction module, which not only reduces features but also inherently provides explainability capabilities.

Yang et al. [15] conducted an extensive benchmark of all 3D MedMNIST datasets, and for comparison purposes, we include their results alongside ours.

### 3.3 Setup

*Hyperparameters* All our models were trained for 50 epochs, using the NAdam optimiser [6], which almost eliminates the need to tune the learning rate. We used a learning rate of  $2 \cdot 10^{-4}$  and a batch size of 64. As a basis for training we utilised a ResNet-18 pretrained on ImageNet [4] and then converted to the respective approach. For the attention pooling and transformer layers we employed eight heads. For training the LSTM RNN feature reduction module we set the hidden size to 128, to limit the number of parameters in this layer. During the first two epochs, we exclusively trained the feature reduction and classification modules, which were randomly initialised. This was done to protect the pre-trained weights from large gradients. After two epochs we also trained the feature extractor.

*Metrics* Consistent with Yang et al. [15], we report the test accuracy (ACC) and area under the receiver-operator curve (AUC) as evaluation metrics.

### 3.4 Experiments

In our first experiment, we evaluated all approaches on all 3D datasets in MedMNIST over five runs with different random seeds. We report the mean metrics in Table 1 and illustrate the results in Figure 2. Notably, our results substantially differ from those reported by Yang [15]. Therefore, we consider our reproductions as the baseline for comparison, as they were trained under identical conditions. Among the baseline methods, the 3D ResNet achieved the best performance but also had the highest number of parameters, demanding substantial computational and time resources. Surprisingly, our framework utilising average pooling as the feature reduction module outperformed other methods on several datasets,

surpassing the next best approach (Synapse dataset) by 9.4% AUC. Interestingly, using a transformer as the reduction method, despite its larger number of parameters and theoretically better learning capabilities, failed to outperform other methods on any dataset. Overall, no single method emerged as superior to others across all datasets. To validate our findings we further evaluated the

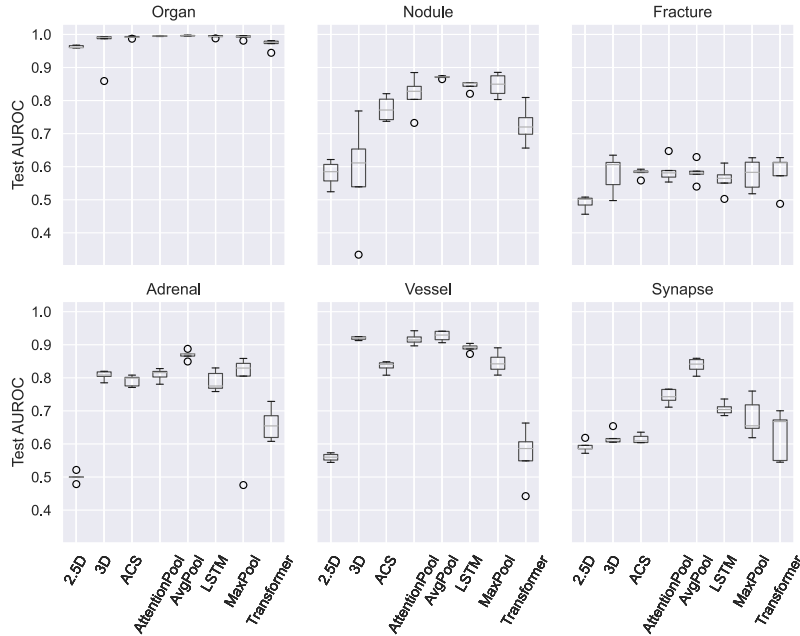


Fig. 2: Boxplots of the test AUC for all MedMNIST3D datasets and all approaches.

approaches on a high-resolution real-world medical imaging dataset of PDAC presence classification. We observed that the ACS approach of [14] and our approach using average pooling, perform best over both metrics. The 3D ResNet as well as our approach using the LSTM or attention pooling all performed on par. The approach using a transformer failed to learn this task.

In addition to classification performance, attention pooling as a feature reduction module introduced inherent explainability by quantifying the weight of each individual slice for 3D data classification. Figure 3 visualises these capabilities of our architecture design. Upon evaluating several examples, we observed that attention was often sparse, with only a small subset of slices receiving the majority of attention weights. Furthermore, there was typically a prominent peak of attention in the patient’s body region, along with noticeable but not negligible attention on slices containing only air. One interesting finding

is that despite achieving over 90% test accuracy, the attention weights were rarely attributed to the tumour or the pancreas.

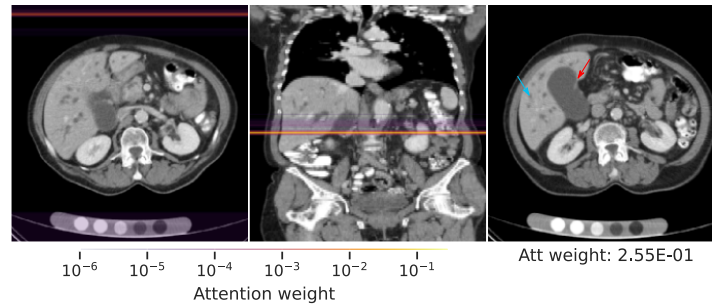


Fig. 3: Exemplary image of a correctly classified PDAC tumour from the test set. The left panel shows the middle axial slice with overlaid attention values of sagittal and coronal slices. The middle panel shows the middle coronal slice with overlaid axial attention values. The right panel shows the slice with highest attention weight. Attention is very sparse and a major part of the slices with non-negligible attention values are on empty parts of the scan. The by far highest attention value is on a slice through the liver, where metastases (blue arrow) and an enlarged gall bladder (red arrow) are seen. Both are strongly indicative of a PDAC.

## 4 Discussion

In our study, we made several noteworthy observations: Firstly, we found that the 3D model did not exhibit a substantial advantage over 2.5D approaches, despite operating in its natural dimension. Secondly, average pooling emerged as the most effective feature reduction method across all datasets, surprising us as we anticipated that meaningless slices could overshadow informative ones. Thirdly, we were surprised by the transformer’s lack of competitive performance compared to other approaches, despite its demonstrated capabilities in previous works, e.g., by Li et al. [9]. We cannot rule out that it is a matter of hyperparameter tuning. Lastly, we discovered that our model predominantly focused on secondary features of tumour patients, such as metastases, rather than the tumour or pancreas themselves.

For future research, it would be valuable to explore the extension of our concept to regression or segmentation tasks. Additionally, validating our finding of what the model pays attention to also transfers to other clinical datasets would be insightful.

In this work, we propose a lightweight and versatile approach that combines various 2D vision models with arbitrary feature reduction modules to create 2.5D architectures. This design facilitates the transfer of information from large pretrainings on 2D vision datasets to 3D data. We demonstrate that it achieves competitive results on several benchmark datasets as well as a real-world clinical dataset. Crucially, our approach can provide inherent explanations for predictions, as the impact of each slice on the final prediction is directly quantifiable.

We hope to contribute to the development of architectures, which are real-world applicable and at the same time not exhibiting the opacity of “black-box” deep learning architectures. We showcase the effectiveness of our approach across various datasets and tasks, providing practitioners with tools to achieve both: competitive performance and explainable results.

## Ethics statement

All subjects gave their informed consent for inclusion before they participated in the study. The study was conducted in accordance with the Declaration of Helsinki, and the protocol was approved by the Ethics Committee of Klinikum Rechts der Isar (180/17S).

## References

1. Antonelli, M., Reinke, A., Bakas, S., Farahani, K., Kopp-Schneider, A., Landman, B.A., Litjens, G., Menze, B., Ronneberger, O., Summers, R.M., et al.: The medical segmentation decathlon. *Nature communications* **13**(1), 4128 (2022)
2. Bai, W., Suzuki, H., Qin, C., Tarroni, G., Oktay, O., Matthews, P.M., Rueckert, D.: Recurrent neural networks for aortic image sequence segmentation with sparse annotations. In: *Medical Image Computing and Computer Assisted Intervention—MICCAI 2018: 21st International Conference, Granada, Spain, September 16–20, 2018, Proceedings, Part IV* 11. pp. 586–594. Springer (2018)
3. Chen, J., Yang, L., Zhang, Y., Alber, M., Chen, D.Z.: Combining fully convolutional and recurrent neural networks for 3d biomedical image segmentation. *Advances in neural information processing systems* **29** (2016)
4. Deng, J., Dong, W., Socher, R., Li, L.J., Li, K., Fei-Fei, L.: Imagenet: A large-scale hierarchical image database. In: *2009 IEEE conference on computer vision and pattern recognition*. pp. 248–255. Ieee (2009)
5. Dosovitskiy, A., Beyer, L., Kolesnikov, A., Weissenborn, D., Zhai, X., Unterthiner, T., Dehghani, M., Minderer, M., Heigold, G., Gelly, S., et al.: An image is worth 16x16 words: Transformers for image recognition at scale. *arXiv preprint arXiv:2010.11929* (2020)
6. Dozat, T.: Incorporating nesterov momentum into adam (2016)
7. He, K., Zhang, X., Ren, S., Sun, J.: Deep residual learning for image recognition. In: *Proceedings of the IEEE conference on computer vision and pattern recognition*. pp. 770–778 (2016)
8. Hochreiter, S., Schmidhuber, J.: Long short-term memory. *Neural computation* **9**(8), 1735–1780 (1997)

9. Li, H., Chen, L., Han, H., Kevin Zhou, S.: Satr: Slice attention with transformer for universal lesion detection. In: Medical Image Computing and Computer Assisted Intervention–MICCAI 2022: 25th International Conference, Singapore, September 18–22, 2022, Proceedings, Part III. pp. 163–174. Springer (2022)
10. Qiu, B., Guo, J., Kraeima, J., Glas, H.H., Zhang, W., Borra, R.J., Witjes, M.J.H., van Ooijen, P.M.: Recurrent convolutional neural networks for 3d mandible segmentation in computed tomography. *Journal of personalized medicine* **11**(6), 492 (2021)
11. Radford, A., Kim, J.W., Hallacy, C., Ramesh, A., Goh, G., Agarwal, S., Sastry, G., Askell, A., Mishkin, P., Clark, J., et al.: Learning transferable visual models from natural language supervision. In: International conference on machine learning. pp. 8748–8763. PMLR (2021)
12. Selvaraju, R.R., Cogswell, M., Das, A., Vedantam, R., Parikh, D., Batra, D.: Grad-cam: Visual explanations from deep networks via gradient-based localization. In: Proceedings of the IEEE international conference on computer vision. pp. 618–626 (2017)
13. Vaswani, A., Shazeer, N., Parmar, N., Uszkoreit, J., Jones, L., Gomez, A.N., Kaiser, Ł., Polosukhin, I.: Attention is all you need. *Advances in neural information processing systems* **30** (2017)
14. Yang, J., Huang, X., He, Y., Xu, J., Yang, C., Xu, G., Ni, B.: Reinventing 2d convolutions for 3d images. *IEEE Journal of Biomedical and Health Informatics* **25**(8), 3009–3018 (2021)
15. Yang, J., Shi, R., Wei, D., Liu, Z., Zhao, L., Ke, B., Pfister, H., Ni, B.: Medmnist v2-a large-scale lightweight benchmark for 2d and 3d biomedical image classification. *Scientific Data* **10**(1), 41 (2023)
16. Zhang, C., Hua, Q., Chu, Y., Wang, P.: Liver tumor segmentation using 2.5 d uv-net with multi-scale convolution. *Computers in Biology and Medicine* **133**, 104424 (2021)
17. Ziller, A., Erdur, A.C., Jungmann, F., Rueckert, D., Braren, R., Kaissis, G.: Exploiting segmentation labels and representation learning to forecast therapy response of pdac patients. In: 2023 IEEE 20th International Symposium on Biomedical Imaging (ISBI) (2023)